ADVANCED ENERGY MATERIALS

www.advenergymat.de

Mechanistic Insights of Zn^{2+} Storage in Sodium Vanadates

Xun Guo, Guozhao Fang, Wenyu Zhang, Jiang Zhou, Lutong Shan, Liangbing Wang, Chao Wang, Tianquan Lin, Yan Tang, and Shuquan Liang**

Rechargeable aqueous zinc-ion batteries (ZIBs) with high safety and low-cost are highly desirable for grid-scale energy storage, yet the energy storage mechanisms in the current cathode materials are still complicated and unclear. Hence, several sodium vanadates with NaV_3O_8-type layered structure (e.g., $Na_5V_{12}O_{32}$ and $HNaV_6O_{16}{\cdot}4H_2O$) and β-$Na_{0.33}V_2O_5$-type tunneled structure (e.g., $Na_{0.76}V_6O_{15}$) are constructed and the storage/release behaviors of Zn^{2+} ions are deeply investigated in these two typical structures. It should be mentioned that the 2D layered $Na_5V_{12}O_{32}$ and $HNaV_6O_{16}{\cdot}4H_2O$ with more effective path for Zn^{2+} diffusion exhibit higher ion diffusion coefficients than that of tunneled $Na_{0.76}V_6O_{15}$. As a result, $Na_5V_{12}O_{32}$ delivers higher capacity than that of $Na_{0.76}V_6O_{15}$, and a long-term cyclic performance up to 2000 cycles at 4.0 A g^{-1} in spite of its capacity fading. This work provides a new perspective of Zn^{2+} storage mechanism in aqueous ZIB systems.

Although current lithium-ion batteries (LIBs) possess high energy density, it is still hard to scale up for grid-scale storage devices due to the limited lithium resources, high-cost, insecurity, and harmful organic electrolyte.[1] As an alternative battery chemistry, rechargeable aqueous zinc-ion batteries (ZIBs) have paved the way not only for realizing environmentally benign and safe energy storage devices, but also reducing the manufacturing costs of next-generation batteries.[2,3] Moreover, the distinctive merits of Zn anode, such as high theoretical capacity (820 mA h g^{-1}), low redox potential (−0.76 V vs standard hydrogen electrode), impressive electrochemical stability in water, high abundance, etc. make the ZIBs a promising battery chemistry for grid-scale energy storage.[4,5]

However, the recent developed cathode materials for aqueous ZIBs still remain challenges, such as prussian blue analogs suffering from low capacity in spite of their stable structure,[6] manganese-based oxides restrained by drastic capacity fading due to the Mn^{2+} dissolution,[7] etc. Therefore, it is urgent to explore the suitable cathodes and boost their electrochemical performance. Unlike the well-established lithium/sodium-ion based energy storage chemistries to storage monovalent alkali metal cations,[8] the reaction mechanisms in aqueous ZIBs system are under debate. For instance, several diverse reaction mechanisms for MnO_2 have been demonstrated: 1) intercalation of Zn^{2+};[9] 2) a conversion reaction mechanism between α-MnO_2 and H^+;[2] and 3) coinsertion of H^+ and Zn^{2+}.[10] For vanadates, Chen and co-workers reported a $NaV_3O_8 \cdot 1.5H_2O$ nanobelt with a simultaneous Zn^{2+} and H^+ insertion/extraction process,[11] which is different from the most reported vanadates experienced the reversible Zn^{2+} intercalation/deintercalation.

Owing to low-cost and the mother open framework of layered V_2O_5, as well as high specific capacity and long-term cyclic performance, vanadium-based materials have been applied as promising cathodes for aqueous ZIBs.[3,4,9,12] Among them, sodium vanadates (NVOs) have captured much attention.[11,13–15] Note that the NVOs involved in this respect are mainly two typical structures (e.g., $NaV_3O_8 \cdot xH_2O$ with layered structure,[14,15] and β-$Na_{0.33}V_2O_5$ with tunneled structure[13]), in which the storage capacity of most cases are induced by the reversible Zn^{2+} intercalation/deintercalation. Structure of NaV_3O_8-type compounds is composed of V_3O_8 polyhedra layers and the inserted sodium ions are mainly located between the layers in the octahedral sites, displaying a typical layered structure (**Figure 1**a),[16] in which the oxygen atoms of layer surface are single-connected and triconnected. β-$Na_{0.33}V_2O_5$ contains tunnels formed by the association of VO_6 octahedra and VO_5 square pyramids along the *b*-axis, in which the inserted sodium ions bonding with single-connected oxygen atoms between the tunnels (Figure 1b).[17] All inserted sodium ions can act as strong "pillars" to stable the whole structure to maintain the structural stability. These different structures and configurations play a key role in the electrochemical properties and their effect on the storage/release behaviors of guest ions is well established

X. Guo, G. Fang, W. Zhang, Prof. J. Zhou, L. Shan, Prof. L. Wang, Prof. Y. Tang, Prof. S. Liang
School of Materials Science and Engineering
Central South University
Changsha 410083, P. R. China
E-mail: zhou_jiang@csu.edu.cn; lsq@csu.edu.cn

Dr. C. Wang, Prof. T. Lin
Department of Nuclear Science and Engineering
Massachusetts Institute of Technology
Cambridge, MA 02139, USA

Prof. T. Lin
State Key Laboratory of High Performance Ceramics and Superfine Microstructure
Shanghai Institute of Ceramics
Chinese Academy of Sciences
Shanghai 200050, P. R. China

The ORCID identification number(s) for the author(s) of this article can be found under https://doi.org/10.1002/aenm.201801819.

DOI: 10.1002/aenm.201801819

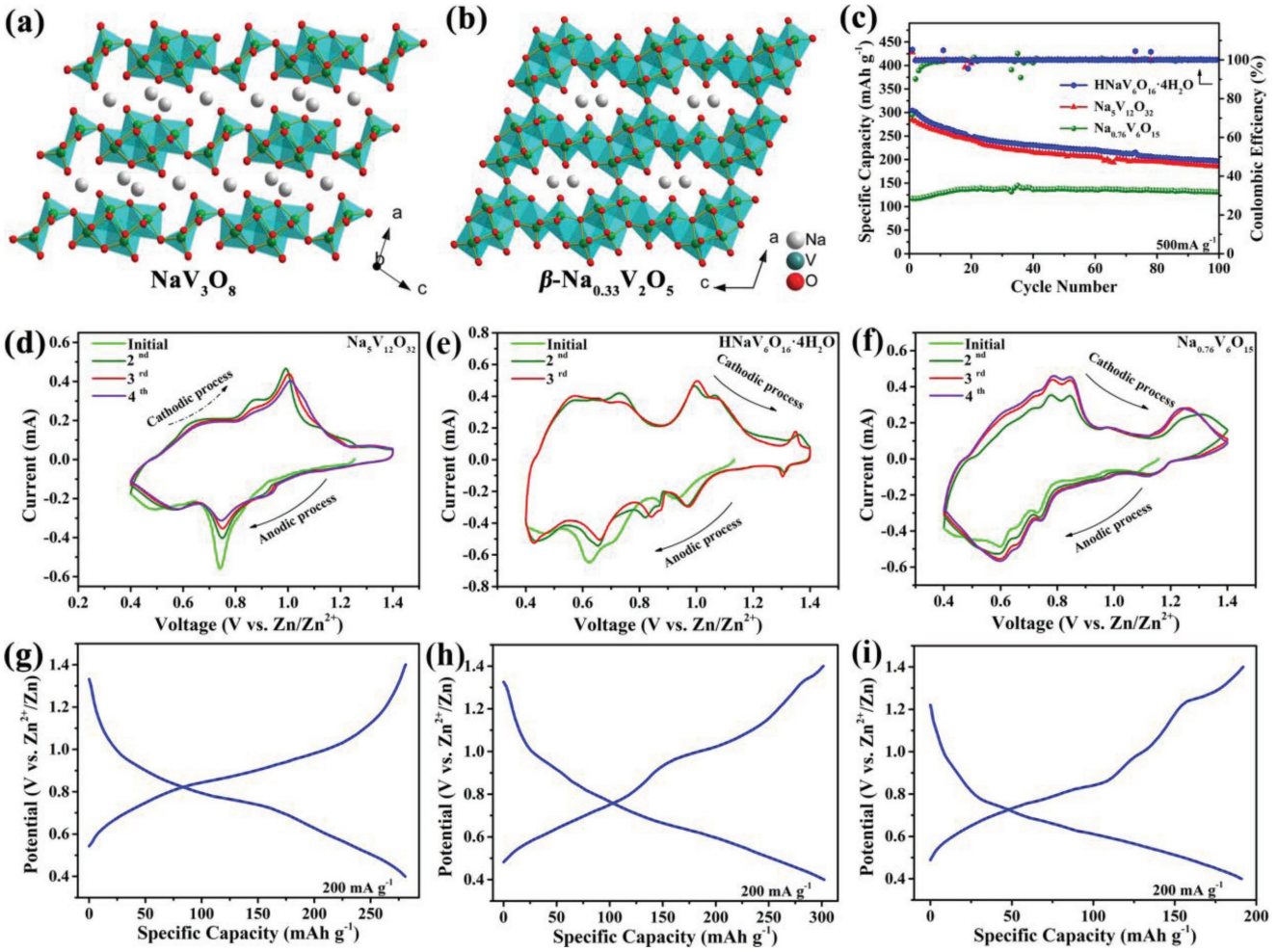

Figure 1. The crystal structure of a) NaV_3O_8, b) β-$Na_{0.33}V_2O_5$. c) Cycling performances at 500 mA g^{-1}, d–f) CV curves at 0.1 mV s^{-1}, and g–i) the charge/discharge curves at 200 mA g^{-1} of $Na_5V_{12}O_{32}$, $HNaV_6O_{16}\cdot 4H_2O$, and $Na_{0.76}V_6O_{15}$.

in LIBs,[18,19] but it has yet been explored for aqueous ZIBs system. A detailed exploration in this respect will accelerate the understanding of current unclear reaction mechanism in aqueous ZIBs.

Here, we purposefully choose and construct three NVOs nanobelts with typical NaV_3O_8-type layered structure, e.g., $Na_5V_{12}O_{32}$ ($Na_{1.25}V_3O_8$), $HNaV_6O_{16}\cdot 4H_2O$ ($H_{0.5}Na_{0.5}V_3O_8\cdot 2H_2O$), and β-$Na_{0.33}V_2O_5$-type tunneled structure, e.g., $Na_{0.76}V_6O_{15}$ ($Na_{0.253}V_2O_5$), and focus on the electrochemical mechanisms of Zn^{2+} storage in these two different structure. The phase and morphology of these NVOs are investigated and shown in Figures S1 and S2 (Supporting Information), indicating high-purity and high-crystallinity of the NVOs nanobelts. Similar storage/release behaviors of Zn^{2+} ions are observed for layered $Na_5V_{12}O_{32}$ and $HNaV_6O_{16}\cdot 4H_2O$, which result in their structural destroy and the formation of the second phase. This phase change may be responsible for their capacity fading, specifically, only 71% capacity retention after 2000 cycles obtained for $Na_5V_{12}O_{32}$. Due to its tunneled structure, $Na_{0.76}V_6O_{15}$ exhibits superior reversible insertion/extraction of Zn^{2+} without structural collapse. Despite its outstanding cycling stability, the ion diffusion coefficients of $Na_{0.76}V_6O_{15}$ are lower than that of NaV_3O_8-type compounds, thus leads to low capacity, e.g., 135 mA h g^{-1} at 0.5 A g^{-1}.

The electrochemical performances of NVOs are evaluated in assembled coin cells (schematized in Figure S3a, Supporting Information). The aqueous ZIBs successfully lit the blue lamp bead shown in Figure S3b (Supporting Information), which indicates the aqueous ZIBs using NVOs as cathode materials can be potential for practical application. As shown in Figure 1c, the $Na_5V_{12}O_{32}$ and $HNaV_6O_{16}\cdot 4H_2O$ electrodes exhibit the similar cyclic performance with high initial capacity of 281 and 304 mA h g^{-1} at 500 mA g^{-1}, respectively, but a gradually degradation in capacity occurs. In contrast, $Na_{0.76}V_6O_{15}$ electrode exhibits an excellent cyclic stability, however, suffers from low capacity (135 mA h g^{-1}). We are motivated by the significant performance diversity in these two typical structures to explore their electrochemical behaviors in detail. The cyclic voltammogram (CV) curves of $Na_5V_{12}O_{32}$, $HNaV_6O_{16}\cdot 4H_2O$, and $Na_{0.76}V_6O_{15}$ are performed at a scan rate of 0.1 mV s^{-1} (Figure 1d–f), depicting a multistep insertion/extraction of Zn^{2+} for all three electrodes, which is also identified by their charge/discharge curves (Figure 1g–i). A representative anodic peak at about 1.0 V

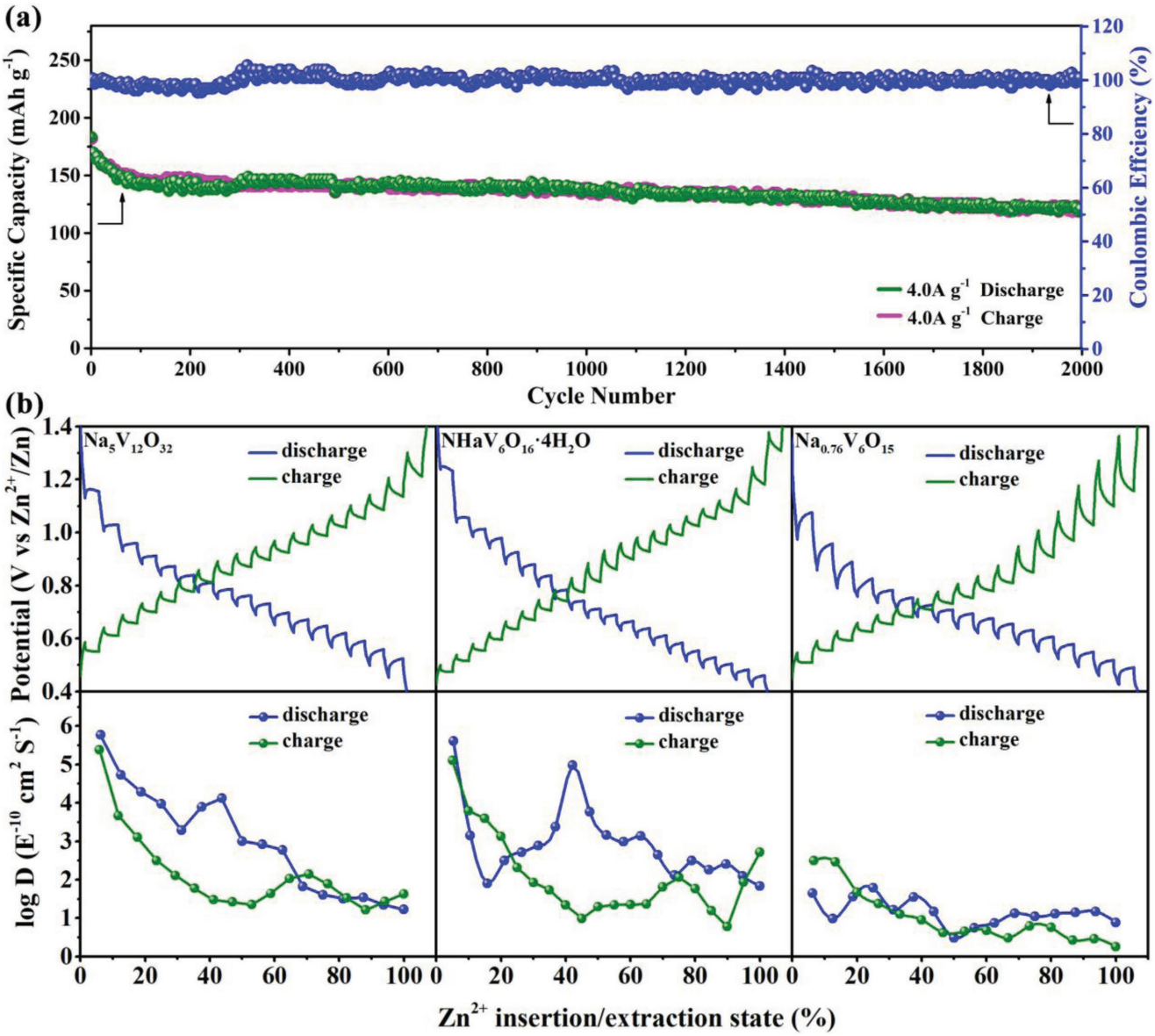

Figure 2. a) Long-term cycling performance at 4 A g^{-1} of $Na_5V_{12}O_{32}$, b) GITT curves and the corresponding Zn^{2+} diffusion coefficient of $Na_5V_{12}O_{32}$, $HNaV_6O_{16}{\cdot}4H_2O$, and $Na_{0.76}V_6O_{15}$.

is observed for $Na_5V_{12}O_{32}$ and $HNaV_6O_{16}{\cdot}4H_2O$, which is also observed in other NaV_3O_8-type compounds.[14,15] But it is absent for $Na_{0.76}V_6O_{15}$ and the reported $Na_{0.33}V_2O_5$.[13] It should be mentioned that the initial redox peaks of $Na_5V_{12}O_{32}$ and $HNaV_6O_{16}{\cdot}4H_2O$ are different from the latter and display a gradually decrease in their intensity corresponding to the capacity fading, while that of $Na_{0.76}V_6O_{15}$ exhibit the similar anodic/cathodic peaks and almost overlap after initial cycle, demonstrating the good reversibility of $Na_{0.76}V_6O_{15}$. The long-cycle measurements further verify that a gradually capacity fading with only 71% and 42% capacity retention after 2000 cycles is observed for $Na_5V_{12}O_{32}$ and $HNaV_6O_{16}{\cdot}4H_2O$, respectively (**Figure 2**a; Figure S4, Supporting Information), but an outstanding cycling stability for $Na_{0.76}V_6O_{15}$ (Figure S5a, Supporting Information). Despite the capacity fading, the $Na_5V_{12}O_{32}$ and $HNaV_6O_{16}{\cdot}4H_2O$ exhibit superior electrochemical performance than that of $Na_{0.76}V_6O_{15}$, e.g., higher capacity and high-rate capacity (Figure S5b, Supporting Information). The same phenomenon of electrochemical performance and capacity fading also can be observed at lower current density (Figure S6, Supporting Information). And the coulombic efficiencies of three different NVOs are around 100% at various current densities, indicating good reversibility of electrodes. It should be noted that the electrochemical performances of these NVOs are far from practical applications, more efforts should be devoted to improve their performances.

The electrochemical reaction kinetics of these NVOs are investigated by the galvanostatic intermittent titration technique (GITT), as shown in Figure 2b. From the plots of discharge process, the overall calculated ion diffusion

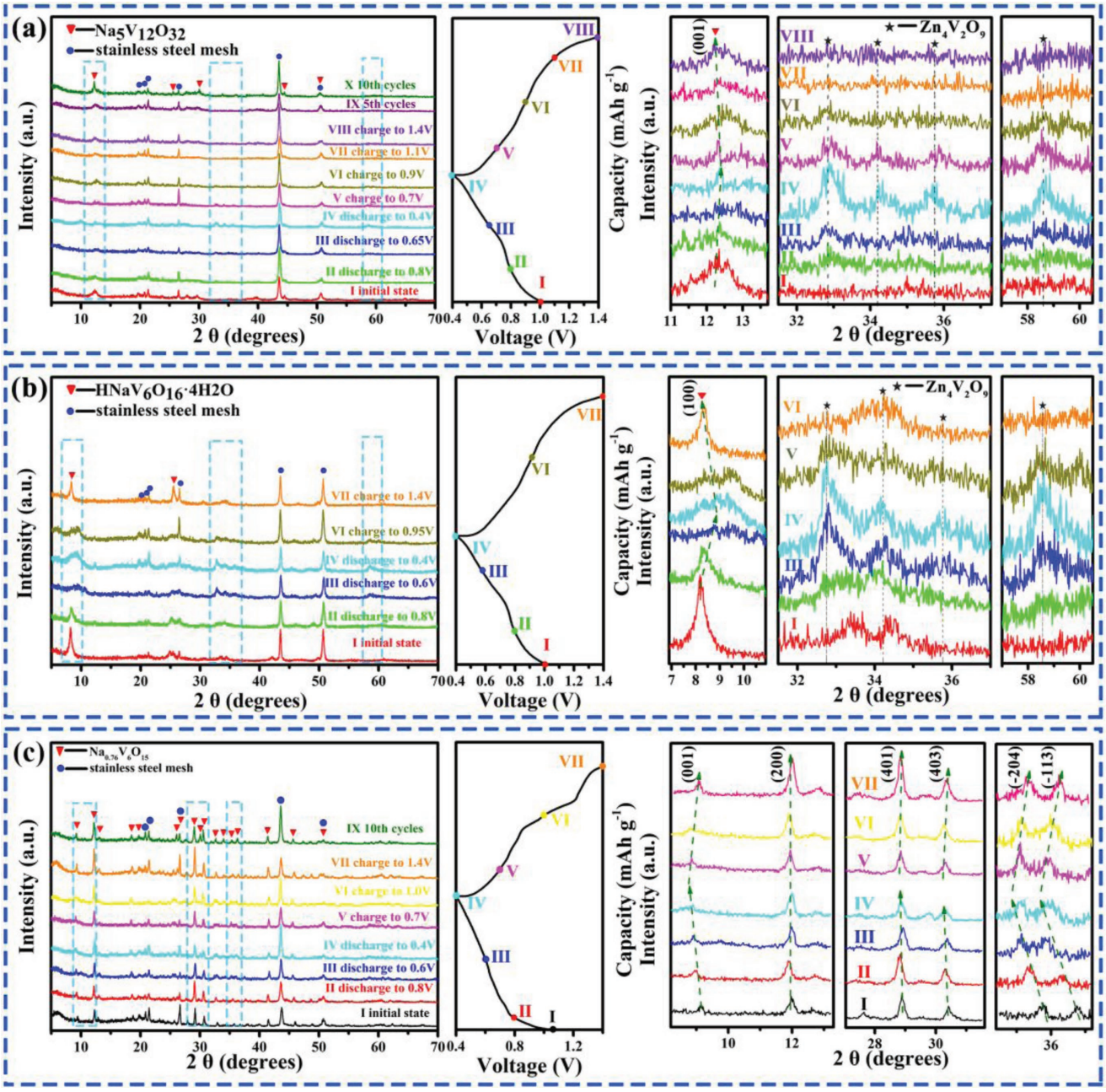

Figure 3. Ex situ XRD patterns at different discharge/charge states of a) $Na_5V_{12}O_{32}$, b) $HNaV_6O_{16}{\cdot}4H_2O$, and c) $Na_{0.76}V_6O_{15}$.

coefficients ($D_{Zn^{2+}}$) of $Na_5V_{12}O_{32}$ and $HNaV_6O_{16}{\cdot}4H_2O$ are higher than that of $Na_{0.76}V_6O_{15}$, because the 2D layered structure with larger lattice spacing may provide more effective diffusion path for Zn^{2+} than the tunneled structure. It should be noted that the ion diffusion coefficient plots of $Na_5V_{12}O_{32}$ and $HNaV_6O_{16}{\cdot}4H_2O$ depict a similar trend that an obvious decrease of $D_{Zn^{2+}}$ occurs after ≈60% insertion of Zn^{2+}. The change of structure may be responsible for this behavior and result in capacity fading, which will be discussed later. In spite of its low values, the $D_{Zn^{2+}}$ of $Na_{0.76}V_6O_{15}$ maintain stable due to the stability of tunneled structure during insertion of Zn^{2+}.

To reveal the internal cause, ex situ XRD is performed to understand the evolution of the structure and phase changes during insertion/extraction of Zn^{2+}. As shown in **Figure 3**a, the diffraction peak of (001) face for $Na_5V_{12}O_{32}$ shifts slightly to higher diffraction angles, indicating the decrease of lattice spacing. We speculate that the divalent Zn^{2+} inserts into the $Na_5V_{12}O_{32}$ host and bonds strongly with vanadium-oxygen layers, thus decrease the lattice spacing of (001) face, which is further supported by related published work.[15] It is reported by Mai and co-workers that the triconnected oxygen atoms existing on the KV_3O_8 layered surface cannot provide strong interaction with the K ions, which results in structural collapse

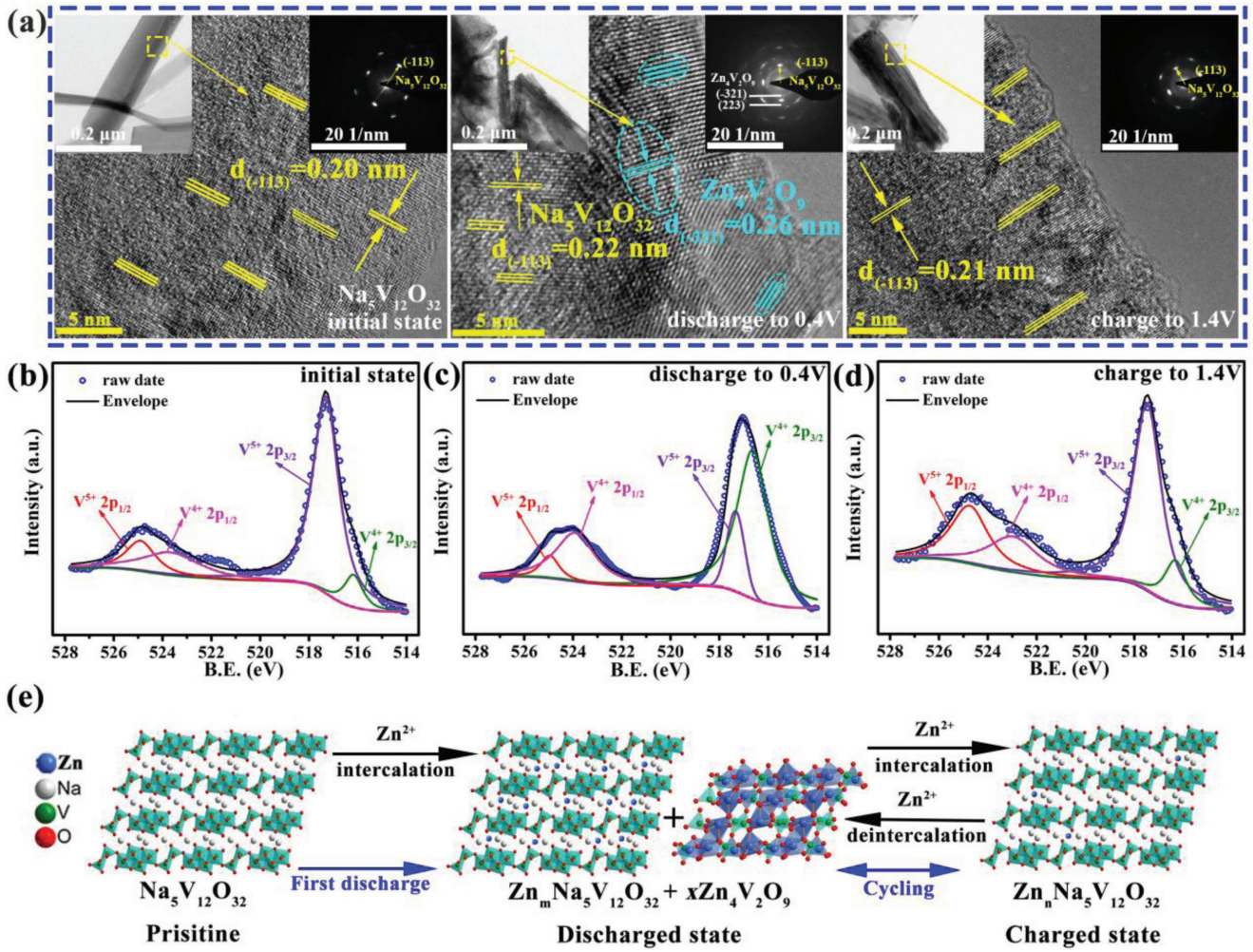

Figure 4. a) Ex situ TEM images at different discharge/charge states of $Na_5V_{12}O_{32}$. b–d) Ex situ high resolution XPS spectrum at different discharge/charge states of $Na_5V_{12}O_{32}$. e) Schematic illustration of Zn^{2+} insertion/extraction process of $Na_5V_{12}O_{32}$ during cycling.

and amorphization during the insertion of Li^+.[19] Note that a decrease in intensity of (001) face during discharge process is observed, and several new peaks gradually appeared at 32.86°, 34.24°, 35.8°, and 58.51°, can be well indexed to $Zn_4V_2O_9$ phase (JCPDS Card No. 77–1757). Therefore, the in-depth insertion of Zn^{2+} into $Na_5V_{12}O_{32}$ leads to the change of the host structure in aqueous ZIBs system, which may account for its capacity fading. During charge process, the diffraction peak of (001) face returns gradually back to its original state, and the new phase disappears, indicating good reversibility of Zn^{2+} storage/release. It is interesting that $HNaV_6O_{16}\cdot 4H_2O$ exhibits a similar electrochemical behavior to $Na_5V_{12}O_{32}$ (Figure 3b). But unlike the NaV_3O_8-type compounds, a quite diverse phenomenon is observed for that of $Na_{0.76}V_6O_{15}$. Except for the shift of some diffraction peaks, it maintains excellent structural stability during initial cycle and even after 10 cycles (Figure 3c; Figure S7, Supporting Information), which verifies its stable tunnel structure.

Ex situ high-resolution transmission electron microscope (HRTEM) and ex situ selected area electron diffraction (SAED) patterns are carried out to further confirm the electrochemical behavior of these NVOs. In the HRTEM image of $Na_5V_{12}O_{32}$ at initial state, the lattice fringes with a spacing of 0.20 nm match well with the (–113) face (**Figure 4**a) with a precise single crystal electron diffraction pattern, demonstrating a single phase. However, it turns to disorder in structure at the fully discharge state with two kinds of lattice fringes which is visible in HRTEM image, corresponding to the SAED pattern, which all can be indexed to (–113) face of $Na_5V_{12}O_{32}$ phase and (–501) of $Zn_4V_2O_9$ phase, respectively. When fully charged, the structure seems to be rearranged into a single phase of $Na_5V_{12}O_{32}$ again, which consistent with the ex situ XRD results, HRTEM image, and SAED pattern. The similar phenomenon observed for $HNaV_6O_{16}\cdot 4H_2O$ (Figure S8, Supporting Information) strongly supports that the insertion of Zn^{2+} into NaV_3O_8-type compounds results in structural destroy accompanied by formation of the second phase (e.g., $Zn_4V_2O_9$). Ex situ HRTEM images of $Na_{0.76}V_6O_{15}$ at different discharge/charge states exhibit the lattice fringe of single phase (Figure S9, Supporting Information), further suggests its excellent structural stability. As discussed above, layered NaV_3O_8 possesses single-connected and triconnected oxygen atoms on the layer surface, while

the tunneled β-$Na_{0.33}V_2O_5$ contains single-connected oxygen atoms. Compared to triconnected oxygen atoms, single-connected oxygen atoms provide stronger interaction with the Na^+, which make it more difficult to be destroyed. In addition, the Zn^{2+} have the smaller radius than that of Na^+ resulting in higher charge density, which make it easier to bond with O^{2-} between the sodium vanadate layers. Therefore, some part of Na^+ in $Na_5V_{12}O_{32}$, which bond with triconnected oxygen atoms, are more likely to be displaced by the Zn^{2+} to form a new phase of $Zn_4V_2O_9$, in which the substituted sodium ions may run off into the $ZnSO_4$ electrolyte. On the country, the Na^+ in $Na_{0.76}V_6O_{15}$ also act as strong "pillars" to stable the whole structure to maintain the good structural stability. To further reveal this issue, we have measured the electrochemical performance of $Na_5V_{12}O_{32}$ using electrolyte of 1 M $ZnSO_4$/1 M Na_2SO_4 and 2 M Na_2SO_4. The CV curves of various electrolytes are performed at a scan rate of 0.1 mV s^{-1} (Figure S10a, Supporting Information). The $ZnSO_4$ electrolyte with/without Na_2SO_4 additive exhibits almost the same CV curve, while no obvious redox peak was observed from the CV curve of the 2 M Na_2SO_4 electrolyte, which is also identified by their charge/discharge curves (Figure S10b, Supporting Information). As a result, electrode in 2 M Na_2SO_4 electrolyte exhibits the ignorable capacity (Figure S10c, Supporting Information), indicating that sodium ions are almost not involved in the redox reaction. It also can be seen that the partial redox peaks of CV curves, located at 0.58, 0.93, and 1 V, is suppressed with the Na_2SO_4 additive, which may be ascribed to that the introduction of Na_2SO_4 can effectively restrain the dissolution of Na^+ ions in the structure of $Na_5V_{12}O_{32}$. As a result, the process of displacement of Na^+ by Zn^{2+} to form a new phase is limited, thus stabilizes the cycling performance but delivers a lower specific capacity (Figure S10c, Supporting Information).

We also give insights into the evolution of valence states for V in $Na_5V_{12}O_{32}$ during cycle, as investigated by X-ray photoelectron spectroscopy (XPS). As shown in Figure 4b, The V $2p_{3/2}$ peak at initial state can be divided into two different peaks located at 516.7 and 517.4 eV, which correspond to V^{4+} $2p_{3/2}$ and V^{5+} $2p_{3/2}$, respectively.[20] The area ratio of V^{5+} to V^{4+} is calculated to be 10.9:1, which is in agreement with the chemical formula of $Na_5V_{12}O_{32}$. After discharged to 0.4 V (Figure 4c), the two peaks become wide and the proportion of V^{4+} $2p_{3/2}$ increases due to the reduction of V^{5+} to V^{4+} during the insertion of Zn^{2+} ions. The area ratio of V^{5+} to V^{4+} of $Na_5V_{12}O_{32}$ is calculated to be 2.2:9.8, corresponding to only a capacity of 190.4 mA h g^{-1}. Hence, the high capacity of 280.3 mA h g^{-1} is obtained for $Na_5V_{12}O_{32}$ as mentioned above, which may be due to the reduction of V^{5+} to V^{4+} and the formation of new phase ($Zn_4V_2O_9$). It should be noted the original area ratio of V^{5+} to V^{4+} in $Na_{0.76}V_6O_{15}$ is calculated to be 5.24:0.76 in Figure S11 of the Supporting Information, but it turns to be 0.73:5.27 at the fully discharged state, corresponding to 214.5 mA h g^{-1}, which is quite close to 220 mA h g^{-1} of $Na_{0.76}V_6O_{15}$ at 100 mA g^{-1} with no new phase generation. The above results also prove that the generation of the new phase contributes a certain capacity. At the fully charge state (Figure 4d), the V 2p spectra almost return to its initial state after the extraction of Zn^{2+}, which is also identified by the high resolution XPS spectra of Zn 2p (Figure S12, Supporting Information) and TEM-EDX element mapping (Figure S13, Supporting Information). Note that there is still a weak signal of Zn, which may be ascribed to the incomplete extraction of Zn^{2+}.

According to the above discussion, the schematic illustration of the reaction mechanisms of NaV_3O_8-type and β-$Na_{0.33}V_2O_5$-type compounds is proposed. In a typical NaV_3O_8-type layered structure, the inserted sodium ions are located between the $(V_3O_8)^-$ layers via a weak van der Waals interaction.[9,21] The intercalation of Zn^{2+} will bond with the unstable V_3O_8 polyhedra layers via a strong electrostatic interaction to decrease the interlayer spacing, and also result in structure destroy. As shown in Figure 4e, during discharge process, Zn^{2+} inserts into the layer of $Na_5V_{12}O_{32}$ to form $Zn_mNa_5V_{12}O_{32}$ and a second phase $Zn_4V_2O_9$ accompanied by the decrease of lattice spacing of (001) face (as indicated in the ex situ XRD in Figure 3a). During charge process, most of Zn^{2+} is extracted from the $Zn_mNa_5V_{12}O_{32}$ and $Zn_4V_2O_9$ compounds, thus turns to Zn_n-$Na_5V_{12}O_{32}$ ($n \ll m$). Upon the subsequent cycles, the Zn^{2+} is reversibly inserted/extracted into/from $Zn_nNa_5V_{12}O_{32}$, indicating the good reversibility of Zn^{2+} storage/release behavior. For $Na_{0.76}V_6O_{15}$, VO_6 octahedra acts as the "pillar" to connect the $[V_6O_{15}]_n$ layers by corner-shared oxygen atoms to change the 2D layered structure into a 3D tunneled structure.[22] Such a rigid structure can effectively alleviate the structure collapse and crystallinity loss during repetitive insertion/extraction of Zn^{2+}. As shown in Figure S14 of the Supporting Information, $Na_{0.76}V_6O_{15}$ exhibits excellent structural stability during cycling.

In summary, we have revealed the different Zn^{2+} storage mechanism in the typical NaV_3O_8-type layered structure and β-$Na_{0.33}V_2O_5$-type tunneled structure. The insertion of Zn^{2+} into NaV_3O_8-type compounds results in structural destroy accompanied by the formation of the second phase, which may be responsible for their capacity fading,, i.e., only 71% capacity retention after 2000 cycles is obtained for $Na_5V_{12}O_{32}$. β-$Na_{0.33}V_2O_5$-type structure exhibits good reversible insertion/extraction of Zn^{2+} without phase changes due to its stable tunneled structure. As a result, $Na_{0.76}V_6O_{15}$ exhibits superior cyclic stability in spite of its low capacity. This finding provides a new perspective of storage/release behaviors of Zn^{2+} storage in sodium vanadates, which provides useful information in the understanding of the unclear reaction mechanism in aqueous ZIBs system.

Supporting Information

Supporting Information is available from the Wiley Online Library or from the author.

Acknowledgements

X.G. and G.F. contributed equally to this work. This work was supported by the National Natural Science Foundation of China (Grant Nos. 51374255, 51302323, and 51572299), Innovation-Driven Project of Central South University (No. 2018CX004), and Hunan Provincial Innovation Foundation for Postgraduate (Grant No. CX2017B045).

Conflict of Interest

The authors declare no conflict of interest.

Keywords

aqueous zinc-ion batteries, layered structure, sodium vanadates, tunneled structure, zinc storage mechanism

Received: June 11, 2018
Revised: July 17, 2018
Published online: August 9, 2018

[1] a) M. Armand, J. M. Tarascon, *Nature* **2008**, *451*, 652; b) V. Etacheri, R. Marom, R. Elazari, G. Salitra, D. Aurbach, *Energy Environ. Sci.* **2011**, *4*, 3243; c) M. S. Whittingham, *Chem. Rev.* **2004**, *104*, 4271; d) J. B. Goodenough, Y. Kim, *Chem. Mater.* **2010**, *22*, 587.

[2] H. Pan, Y. Shao, P. Yan, Y. Cheng, K. S. Han, Z. Nie, C. Wang, J. Yang, X. Li, P. Bhattacharya, K. T. Mueller, J. Liu, *Nat. Energy* **2016**, *1*, 16039.

[3] D. Kundu, B. D. Adams, V. Duffort, S. H. Vajargah, L. F. Nazar, *Nat. Energy* **2016**, *1*, 16119.

[4] C. Xia, J. Guo, P. Li, X. Zhang, H. N. Alshareef, *Angew. Chem., Int. Ed.* **2018**, *57*, 3943.

[5] F. Wang, O. Borodin, T. Gao, X. Fan, W. Sun, F. Han, A. Faraone, J. A. Dura, K. Xu, C. Wang, *Nat. Mater.* **2018**, *17*, 543.

[6] a) L. Zhang, L. Chen, X. Zhou, Z. Liu, *Adv. Energy Mater.* **2015**, *5*, 1400930; b) Z. Jia, B. Wang, Y. Wang, *Mater. Chem. Phys.* **2015**, *149–150*, 601.

[7] a) N. Zhang, F. Cheng, Y. Liu, Q. Zhao, K. Lei, C. Chen, X. Liu, J. Chen, *J. Am. Chem. Soc.* **2016**, *138*, 12894; b) C. Xu, B. Li, H. Du, F. Kang, *Angew. Chem.* **2012**, *124*, 957; c) S.-D. Han, S. Kim, D. Li, V. Petkov, H. D. Yoo, P. J. Phillips, H. Wang, J. J. Kim, K. L. More, B. Key, R. F. Klie, J. Cabana, V. R. Stamenkovic, T. T. Fister, N. M. Markovic, A. K. Burrell, S. Tepavcevic, J. T. Vaughey, *Chem. Mater.* **2017**, *29*, 4874; d) B. Jiang, C. Xu, C. Wu, L. Dong, J. Li, F. Kang, *Electrochim. Acta* **2017**, *229*, 422; e) C. Zhu, G. Fang, J. Zhou, J. Guo, Z. Wang, C. Wang, J. Li, Y. Tang, S. Liang, *J. Mater. Chem. A* **2018**, *6*, 9677; f) M. H. Alfaruqi, V. Mathew, J. Gim, S. Kim, J. Song, J. P. Baboo, S. H. Choi, J. Kim, *Chem. Mater.* **2015**, *27*, 3609; g) W. Sun, F. Wang, S. Hou, C. Yang, X. Fan, Z. Ma, T. Gao, F. Han, R. Hu, M. Zhu, C. Wang, *Chem. Soc.* **2017**, *139*, 9775.

[8] a) M. R. Palacin, *Chem. Soc. Rev.* **2009**, *38*, 2565; b) J. Meng, H. Guo, C. Niu, Y. Zhao, L. Xu, Q. Li, L. Mai, *Joule* **2017**, *1*, 522; c) G. Fang, Z. Wu, J. Zhou, C. Zhu, X. Cao, T. Lin, Y. Chen, C. Wang, A. Pan, S. Liang, *Adv. Energy Mater.* **2018**, *8*, 1703155.

[9] M. H. Alfaruqi, V. Mathew, J. Song, S. Kim, S. Islam, D. T. Pham, J. Jo, S. Kim, J. P. Baboo, Z. Xiu, K.-S. Lee, Y.-K. Sun, J. Kim, *Chem. Mater.* **2017**, *29*, 1684.

[10] W. Sun, F. Wang, S. Hou, C. Yang, X. Fan, Z. Ma, T. Gao, F. Han, R. Hu, M. Zhu, C. Wang, *J. Am. Chem. Soc.* **2017**, *139*, 9775.

[11] F. Wan, L. Zhang, X. Dai, X. Wang, Z. Niu, J. Chen, *Nat. Commun.* **2018**, *9*, 1656.

[12] a) M. Yan, P. He, Y. Chen, S. Wang, Q. Wei, K. Zhao, X. Xu, Q. An, Y. Shuang, Y. Shao, K. T. Mueller, L. Mai, J. Liu, J. Yang, *Adv. Mater.* **2018**, *30*, 1703725; b) C. Xia, J. Guo, Y. Lei, H. Liang, C. Zhao, H. N. Alshareef, *Adv. Mater.* **2018**, *30*, 1705580; c) Y. Cai, F. Liu, Z. Luo, G. Fang, J. Zhou, A. Pan, S. Liang, *Energy Storage Mater.* **2018**, *13*, 168; d) J. Zhou, L. Shan, Z. Wu, X. Guo, G. Fang, S. Liang, *Chem. Commun.* **2018**, *54*, 4457; e) C. Xia, J. Guo, P. Li, X. Zhang, H. N. Alshareef, *Angew. Chem. Int. Ed.* **2018**, *57*, 3943; f) W. Kaveevivitchai, A. J. Jacobson, *Chem. Mater.* **2016**, *28*, 4593; g) C. Xia, J. Guo, Y. Lei, H. Liang, C. Zhao, H. N. Alshareef, *Adv. Mater.* **2018**, *30*, 1705580; h) P. He, M. Yan, G. Zhang, R. Sun, L. Chen, Q. An, L. Mai, *Adv. Energy Mater.* **2017**, *7*, 1601920; i) P. Hu, M. Yan, T. Zhu, X. Wang, X. Wei, J. Li, L. Zhou, Z. Li, L. Chen, L. Mai, *ACS Appl. Mater. Interfaces* **2017**, *9*, 42717; j) C. Xia, J. Guo, P. Li, X. Zhang, H. N. Alshareef, *Angew. Chem., Int. Ed.* **2018**, *57*, 3943.

[13] P. He, G. Zhang, X. Liao, M. Yan, X. Xu, Q. An, J. Liu, L. Mai, *Adv. Energy Mater.* **2018**, *8*, 1702463.

[14] P. Hu, T. Zhu, X. Wang, X. Wei, M. Yan, J. Li, W. Luo, W. Yang, W. Zhang, L. Zhou, Z. Zhou, L. Mai, *Nano Lett.* **2018**, *18*, 1758.

[15] V. Soundharrajan, B. Sambandam, S. Kim, M. H. Alfaruqi, D. Y. Putro, J. Jo, S. Kim, V. Mathew, Y. K. Sun, J. Kim, *Nano Lett.* **2018**, *18*, 2402.

[16] Y. Dong, S. Li, K. Zhao, C. Han, W. Chen, B. Wang, L. Wang, B. Xu, Q. Wei, L. Zhang, X. Xu, L. Mai, *Energy Environ. Sci.* **2015**, *8*, 1267.

[17] a) R. Baddour-Hadjean, S. Bach, N. Emery, J. P. Pereira-Ramos, *J. Mater. Chem.* **2011**, *21*, 11296; b) J. K. Kim, B. Senthilkumar, S. H. Sahgong, J. H. Kim, M. Chi, Y. Kim, *ACS Appl. Mater. Interfaces* **2015**, *7*, 7025.

[18] Y. Zhao, C. Han, J. Yang, J. Su, X. Xu, S. Li, L. Xu, R. Fang, H. Jiang, X. Zou, B. Song, L. Mai, Q. Zhang, *Nano Lett.* **2015**, *15*, 2180.

[19] J. Meng, Z. Liu, C. Niu, X. Xu, X. Liu, G. Zhang, X. Wang, M. Huang, Y. Yu, L. Mai, *J. Mater. Chem. A* **2016**, *4*, 4893.

[20] G. A. Sawatzky, D. Post, *Phys. Rev. B* **1979**, *20*, 1546.

[21] a) F. Wang, X. Wang, Z. Chang, Y. Zhu, L. Fu, X. Liu, Y. Wu, *Nanoscale Horiz.* **2016**, *1*, 272; b) N. A. Chernova, M. Roppolo, A. C. Dillon, M. S. Whittingham, *Mater. Chem.* **2009**, *19*, 2526.

[22] D. Sun, G. Jin, H. Wang, P. Liu, Y. Ren, Y. Jiang, Y. Tang, X. Huang, *J. Mater. Chem. A* **2014**, *2*, 12999.

